

OPEN ACCESS

LiCl-Based Aqueous Electrolytes for Efficient Iron Electrodeposition

To cite this article: William Lvovich *et al* 2025 *J. Electrochem. Soc.* **172** 110503

View the [article online](#) for updates and enhancements.

You may also like

- [Unveiling the Dependent Relationship of Dendrite Metrics on Separator Thermophysical Parameters: A Phase-Field Study](#)
Yajie Li, Mengyang Xu, Yuxiao Lin et al.
- [Ni_{0.5}Co_{0.5}S₂ Cathode for Thermal Batteries: Examination of High-Temperature Discharge Characteristics and Phase Transition Mechanisms](#)
Xuefeng Chen, Licheng Tang, Jun Tang et al.
- [Heterogeneity Disparities in Electrodes and Their Effect on Lithium-Ion Cell Performance: A Dual Electrode Study with Integrated Machine Learning](#)
Md. Faizan and Obaidallah Munteshari

Your Lab in a Box!

The PAT-Tester-i-16 Multi-Channel Potentiostat for Battery Material Testing!

- ✓ **All-in-One Solution with Integrated Temperature Chamber (+10 to +80 °C)!**
No additional devices are required to measure at a stable ambient temperature.
- ✓ **Fully Featured Multi-Channel Potentiostat / Galvanostat / EIS!**
Up to 16 independent battery test channels, no multiplexing.
- ✓ **Ideally Suited for High-Precision Coulometry!**
Measure with excellent accuracy and signal-to-noise ratio.
- ✓ **Small Footprint, Easy to Setup and Operate!**
Cableless connection of 3-electrode battery test cells. Powerful EL-Software included.



EL-CELL[®]
electrochemical test equipment

Learn more on our product website:



Download the data sheet (PDF):



Or contact us directly:

+49 40 79012-734

sales@el-cell.com

www.el-cell.com



LiCl-Based Aqueous Electrolytes for Efficient Iron Electrodeposition

William Lvovich,^{1,2,*} Nicholas Sinclair,^{1,2} Justin G. Connell,^{2,3} and Rohan Akolkar^{1,2,*,z}

¹Department of Chemical and Biomolecular Engineering, Case Western Reserve University, Cleveland, Ohio, 44106, United States of America

²Center for Steel Electrification by Electrosynthesis, Argonne National Laboratory, Lemont, Illinois 60439, United States of America

³Materials Science Division, Argonne National Laboratory, Lemont, Illinois, 60439, United States of America

This study investigates room temperature, aqueous electrolytes for efficient iron electrodeposition. Specifically, a novel lithium chloride-based electrolyte was identified to suppress hydrogen evolution while promoting fast kinetics of iron electrodeposition, achieving high coulombic efficiency (>90%) at high current densities (>400 mA cm⁻²). Electrochemical analysis of the partial current densities of iron deposition and hydrogen co-evolution revealed that water reduction is kinetically suppressed in this electrolyte, resulting in an increase in the measured coulombic efficiency. Furthermore, a detailed investigation of the iron speciation and their complexation was performed, which revealed that, in concentrated LiCl-containing electrolytes, the ferrous (Fe²⁺) species coordinate with chloride rather than water, enhancing deposition kinetics. The combined effect of enhanced electrodeposition kinetics and suppressed water activity provide elevated coulombic efficiency. Overall, this paper develops an understanding of anion and cation effects on the mechanism of electrodeposition and hydrogen co-evolution in concentrated electrolytes in search of improved aqueous media (e.g., concentrated LiCl) for efficient metal electro-synthesis.

© 2025 The Author(s). Published on behalf of The Electrochemical Society by IOP Publishing Limited. This is an open access article distributed under the terms of the Creative Commons Attribution 4.0 License (CC BY, <https://creativecommons.org/licenses/by/4.0/>), which permits unrestricted reuse of the work in any medium, provided the original work is properly cited. [DOI: 10.1149/1945-7111/ae16dd]



Manuscript submitted August 7, 2025; revised manuscript received October 6, 2025. Published November 3, 2025.

List of Symbols

Symbol	Description	Units
i_{Fe}	Iron partial current density	mA/cm ²
$i_{\text{H}_2\text{O}}$	Water reduction partial current density	mA/cm ²
i_{Total}	Total current density	mA/cm ²
i_{H}	Proton reduction current density	mA/cm ²
ϵ	Coulombic efficiency	—
i	Current density	mA/cm ²
$i_{0,\text{Fe}}$	Iron plating exchange current density	mA/cm ²
E_0	Standard reduction potential	V vs SHE
E_{Fe}	Iron reduction equilibrium potential	V vs SHE
α_c	Cathodic charge transfer coefficient	—
F	Faraday's constant	C/mol
R_Ω	Ohmic resistance	Ω cm ²
R	Universal gas constant	J/mol-K
T	Temperature	K
$E_{\text{H}_2\text{O}}$	Water reduction equilibrium potential	V vs SHE
V	Applied potential	V vs SHE
$i_{0,\text{H}_2\text{O}}$	Water reduction exchange current density	mA/cm ²
$i_{\text{L,Fe}}$	Iron plating limiting current density	mA/cm ²
η	Overpotential	V
n	Number of electrons	—
D	Diffusion coefficient	cm ² /s

Iron and steel manufacturing make up approximately 95% of global metal production.¹ The primary industrial reactor for processing iron ore into iron metal is the conventional blast furnace.² Despite the fact that a blast furnace delivers a homogenous and high purity iron product, the high equipment costs and energy consumption^{3,4} call for a more modular, cost-effective alternative. Due to these constraints, major consumers of iron and steel such as the United States have begun to transition to electric arc furnaces (EAF), and about 70% of their annual steel production comes from

EAF steel recycling.⁴ However, this does not address the unmet need for increased primary iron production directly from ore. Electrochemical iron production has the potential to become a cost-effective, modular alternative to the blast furnace because of its potential to lower energy consumption.⁵ Several methods of electrochemical production of iron are currently being pursued. Molten oxide electrolysis (MOE) converts pure iron oxide into iron and oxygen gas at a high coulombic efficiency and rate,⁶ but due to its high operating temperature (1600 °C), MOE faces various challenges ranging from material compatibility issues⁷ to the development of an industrially viable oxygen evolving anode.^{8–10} Alternatively, chloride-based molten salt electrolysis (CMSE) electrodeposits iron from a mixture of chloride salts at moderate temperatures (~500 °C) and at high efficiencies and operating rates.^{5,11} One of CMSE's most attractive features is that low grade ores such as taconite⁵ can be separated and converted into a usable salt for electrolysis through non-carbothermic chlorination, providing an industrial use for an admittedly low-quality feedstock.

Despite progress in the development of novel molten salt-based electrolysis technologies, aqueous electrochemistry remains an attractive approach for iron electrowinning as it is a safe, low temperature route with the potential to be a cost-effective alternative to blast furnace production of iron. However, the parasitic hydrogen evolution reaction (HER) in water significantly lowers the coulombic efficiency of iron electrodeposition in an aqueous electrolyte.¹² Therefore, for practical use of aqueous electrolytes in electrowinning, it is crucial to suppress HER while not sacrificing other key metrics such as electrolyte stability and high deposition rates. From a pure Fe₂O₃ feedstock, SiDERWIN¹³ and Konovalova et al.¹⁴ have both investigated aqueous Fe₂O₃ reduction in an alkaline electrolyte. Konovalova et al. reported a wide range of weight based coulombic efficiencies (60%–90%) for slurries of 98% pure α -Fe₂O₃ that were suspended in 10 M NaOH at current densities approaching 800 mA cm⁻². However, realistic iron ore powders result in significantly reduced efficiencies via this approach.¹⁵ In another approach, Electra¹⁶ utilizes acid dissolution followed by electrolysis at low pH and near ambient temperatures.^{17–19} The technology proposed by Electra is reported to operate at current densities of ~100 mA cm⁻² and the two iron reduction reactions (Fe³⁺→Fe²⁺ and Fe²⁺→Fe⁰) are separated into isolated electrochemical cells resulting in an efficient but potentially

*Electrochemical Society Student Member.

**Electrochemical Society Fellow.

^zE-mail: RNA3@case.edu

capital intensive process.¹⁸ Ore leaching, Fe³⁺ reduction, and oxygen evolution all occur within Electra's dissolution cell.¹⁸ An ideal, single cell system would leach the ore before addition to the cell, to ensure constant electrolyte composition, while electrochemically reducing iron (Fe³⁺ → Fe⁰) in one step.

One alternative to suppress HER while maintaining high current density is to utilize water-in-salt electrolytes (WiSE), which were initially developed for use in lithium-ion batteries.²⁰ WiSE can be simply understood as highly concentrated solutions that alter the coordination chemistry of water to suppress its electrolysis to H₂.²¹ WiSE media are attractive for their ability to suppress hydrogen evolution and broaden the practical electrochemical stability window of an aqueous electrolyte while maintaining a high concentration of both charge carriers and electro-active species. Several attempts to incorporate WiSE principles into iron electrodeposition demonstrate that these electrolytes have several shortcomings, such as inability to achieve high ionic conductivity, instability issues resulting from operating at a natural pH, and operation limited to current densities under 1 mA cm⁻².^{22,23} Previous work done at CWRU investigated choline chloride (ChCl)-based WiSE like electrolytes with moderate conductivities (50 mS cm⁻¹).²⁴ The ChCl system achieved a respectable coulombic efficiency (~85%) for iron plating at moderate current densities (50 mA cm⁻²). However, the Ch⁺ exhibited active hydrogen bond donor interactions, forcing the Fe²⁺ ion into a bulkier complex, hindering its diffusion. Therefore, it is expected that a smaller, non-hydrogen bonding alkali cation may exhibit increased conductivity and decreased viscosity while still suppressing HER. Bender et al.²⁵ investigated the effect of alkali metal cations on HER in both acidic and alkaline media on noble and reactive metal substrates. They found that the cation type had no effect on HER from proton reduction in acidic medium. However, on noble metal electrodes (Cu, Ag, Au) in an alkaline environment, the rate of HER increased with increasing cation size (Li⁺ < Na⁺ < K⁺ < Cs⁺) due to larger cations' tendency to interact with the electrode surface. This is due to the larger, weakly hydrated cations' ability to partially lose their solvation allowing for an easier approach to the electrode surface.^{25–27} Bender et al. report that these larger interfacial cations lower the activation barrier for the rate-limiting water dissociation step, increasing the net HER rate. Therefore, on noble metals, the larger cations facilitate water dissociation, whereas Li⁺ strongly coordinates with water which will either prevent water reaching the electrode or ensure sluggish HER kinetics on a noble metal electrode.²⁸ Considering the anion effect on the deposition reaction, Hawthorne et al.²⁹ showed that chloride improves iron deposition kinetics while decreasing the HER rate when compared to a sulfate electrolyte due to surface adsorption effects.

Aqueous, room temperature electrolytes with careful cation and anion selection paired with an understanding of concentration effects has the potential to offer efficient electrolytic iron production at high current densities. In this work, we illustrate how increasing lithium chloride (LiCl) concentrations in aqueous media improves both the coulombic efficiency and operating current density during iron deposition. We investigate the specific role of cationic and anionic species in iron complexation, and their impacts on the iron deposition reaction and associated HER kinetics from both proton and water reduction. This work highlights the importance of careful anion and cation selection in designing the supporting electrolyte, and integrates WiSE principles to achieve highly efficient electrodeposition of iron metal.

Experimental

All LiCl electrolytes were prepared from deionized water, iron (II) chloride tetrahydrate (FeCl₂, 99% purity, Thermo Scientific), lithium chloride (LiCl, 99% purity, Thermo Scientific), and hydrochloric acid (HCl, 37% assay, Fisher Scientific). Electrolytes consist of 1 M FeCl₂, 0.01 M HCl and 1–6 M LiCl as designated.

Electrochemical measurements, done at ambient temperature (≈22 °C), were performed with a Gamry 1010 potentiostat using a

rotating disk electrode (RDE) from Pine Research with a 5 mm copper disk working electrode, a Ag/AgCl (4 M KCl) reference electrode from BASi, and a graphite rod counter electrode on which Fe²⁺ oxidation occurred. The duration of experiments was typically short ensuring no Fe³⁺ build up in the cell. Electrochemical impedance measurements provided the solution resistance for overpotential calculations. Stripping coulometry was performed at 1000 RPM. Here, iron deposition was performed galvanostatically for 20 s, and then stripped under potentiostatic conditions at –0.2 V vs Ag/AgCl until the current decayed to <100 μA. The coulombic efficiency was calculated by dividing the total charge measured during stripping (Q_{strip}) by the total charge passed during plating (Q_{plate}). Slow scan polarization was performed on the copper disk RDE at 1000 RPM and at a potential scan rate of 5 mV s⁻¹. Iron (Fe²⁺) species diffusion coefficients were determined on a 4 mm glassy carbon RDE using Levich analysis of the diffusion-limited Fe²⁺ oxidation currents at variable rotation rates (500–2500 RPM).

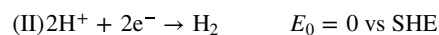
Electrochemical experiments were replicated on a set of comparative electrolytes prepared from: (i) deionized water, iron (II) perchlorate hexahydrate (Fe(ClO₄)₂, 99% purity, Alfa Aesar), lithium perchlorate trihydrate (LiClO₄, 99% purity, Stern Chemicals), and perchloric acid (HClO₄, 70% assay, Fisher Scientific); and (ii) deionized water, iron (II) chloride tetrahydrate (FeCl₂, 99% purity, Thermo Scientific), potassium chloride (KCl, 99% purity, Thermo Scientific), and hydrochloric acid (HCl, 37% assay, Fisher Scientific). Electrolyte (i) consisted of 1 M FeClO₄, 0.01 M HClO₄, and 3 M LiClO₄. Electrolyte (ii) consisted of 1 M FeCl₂, 0.01 M HCl, and 3 M KCl.

A computational approach similar to the one described by Shen et al.³⁰ for copper complexation was performed to calculate iron coordination species concentrations as a function of the total chloride concentration. For this calculation, iron species stability constants were obtained from Zhao et al.³¹

Results and Discussion

Measuring plating efficiency and partial currents.—Ensuring that parasitic side reactions (i.e., HER) are suppressed in comparison to the desired Fe electrodeposition reaction is vital to enabling efficient deposition of Fe metal. To understand the effects of LiCl concentration on the Fe plating coulombic efficiency, stripping coulometry was performed on a Cu RDE. The hydrodynamic conditions at the RDE ensure that the generated hydrogen gas is swept away from the electrode surface and does not “block” the deposited metal. This also ensures that the measured oxidative current is related to iron stripping. Coulombic efficiency measurements (Fig. 1) were performed in 1, 3, 5 and 6 M LiCl electrolytes, each containing 1 M FeCl₂ and 0.01 M HCl. Regimes 1, 2 and 3 in Fig. 1 correspond to low current densities (<100 mA cm⁻²), moderate current densities (100–400 mA cm⁻²), and high current densities (>400 mA cm⁻²) respectively.

To interpret trends observed in these regimes of Fig. 1, we must first understand the reactions occurring at the electrode. The changes in efficiency in Fig. 1 represents a competition between the iron deposition and parasitic hydrogen evolution (HER). These reactions and their standard redox potential³² are:



In regime 1, at low current densities and thus correspondingly low applied overpotentials, the iron deposition reaction (I) competes primarily with hydrogen evolution from proton reduction (II). In this case, the coulombic efficiency increases with both increasing LiCl concentration and current density. This is expected because HER from proton reduction rapidly reaches its limiting current on account

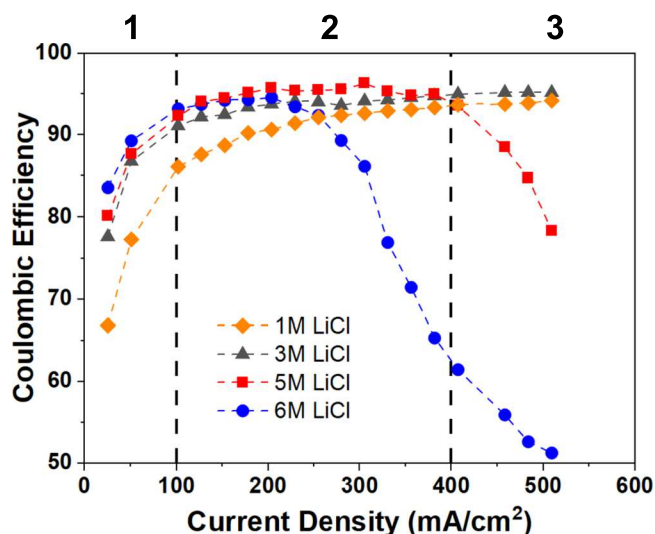


Figure 1. Coulombic efficiencies for Fe plating as a function of current density for electrolytes containing 1 M FeCl_2 , 0.01 M HCl and increasing concentrations of LiCl. Three distinct regimes (labelled 1, 2, and 3) with characteristic dependence of efficiency on current density are noted.

of the low H^+ concentrations.²⁴ Also, it has been reported that at higher concentrations of LiCl, reaction (II) is actively suppressed because LiCl disrupts the Grotthuss mechanism lowering proton

diffusion and correspondingly its limiting current.^{29,33} These effects result in enhanced iron plating relative to proton reduction as the applied current density is increased or the LiCl concentration is increased in regime 1, showing up as an increase in coulombic efficiency.

In regime 2 of Fig. 1, the electrode potential is sufficiently negative to produce hydrogen from direct water reduction via reaction (III). This results in a competition between the deposition reaction (I) and hydrogen evolution from proton reduction (II) and now additionally the breakdown of water (III). The competition results in the coulombic efficiency increasing as the LiCl concentration increases from 1 M to 5 M; however, above 200 mA cm^{-2} , the 6 M LiCl electrolyte has a significant decline in coulombic efficiency. As discussed later, this is explained by the Fe^{2+} species experiencing mass transport limitations, thereby triggering substantial water reduction. The 5 M LiCl is the best performing electrolyte in regime 2, which reaches a coulombic efficiency of 95% at current densities ranging between 200 to 400 mA cm^{-2} . The reliability of this coulometrically-obtained efficiency data was confirmed via gravimetric analysis of Fe deposits obtained after 5 min of plating for the 5 M LiCl electrolyte at 250 mA cm^{-2} , which provided a coulombic efficiency of 94.8% via Faraday's law, matching the coulometric efficiency.

In regime 3, water reduction becomes a larger portion of the total current as the electrode potential becomes even more negative. For 5 M LiCl, the iron deposition also approaches its limiting current, which decreases the overall Fe plating efficiency. Interestingly, in this region, electrolytes with 3 M LiCl exhibit the highest coulombic

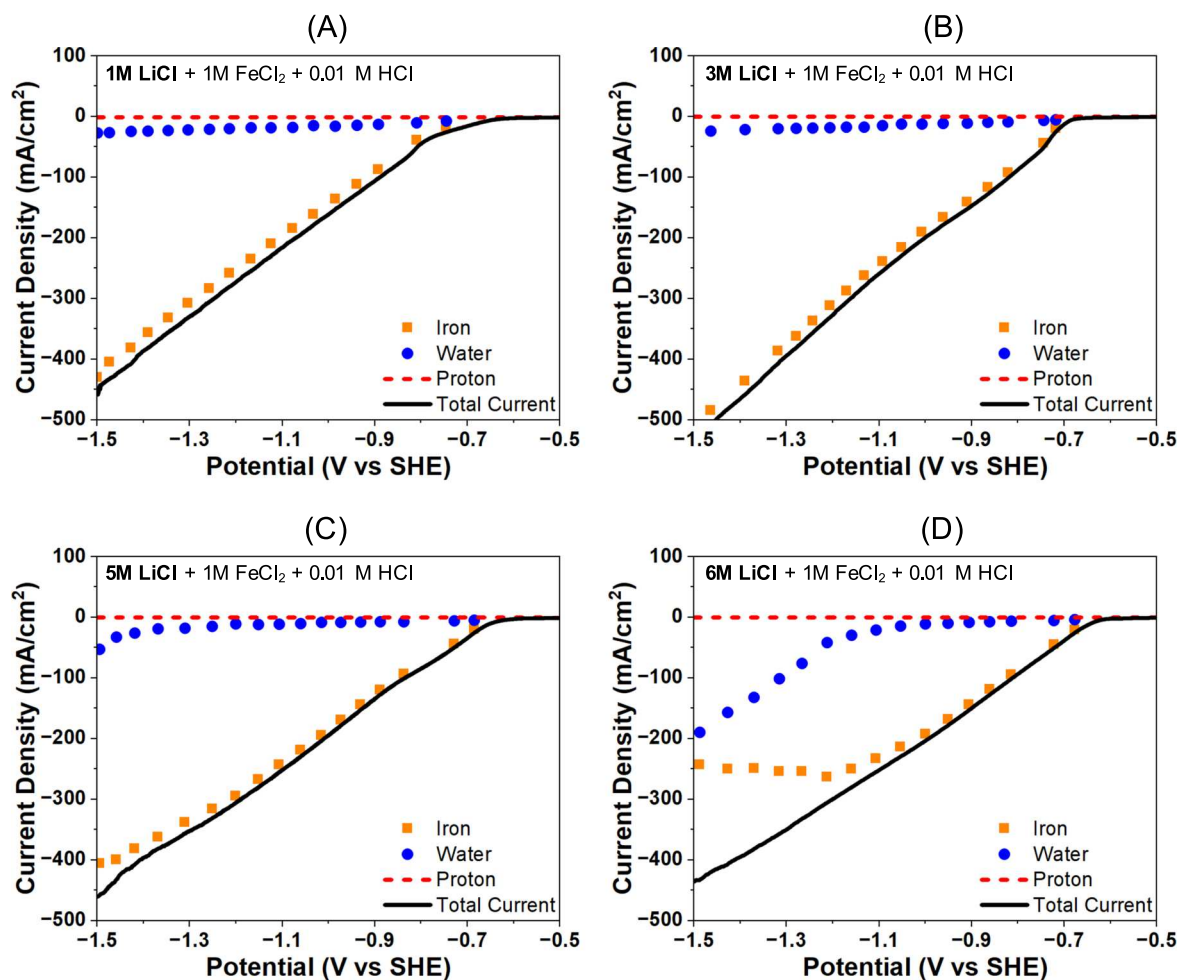


Figure 2. Deconvoluting polarization behavior into partial currents for iron deposition (i_{Fe}), water reduction ($i_{\text{H}_2\text{O}}$), and proton reduction (i_{H}) for electrolytes containing 1 M FeCl_2 and 0.01 M HCl in the presence of various LiCl concentrations of 1 M (A), 3 M (B), 5 M (C), 6 M (D). $i_{\text{H}_2\text{O}}$ is small compared to i_{Fe} until mass transport limitations are imposed on i_{Fe} at 6 M LiCl.

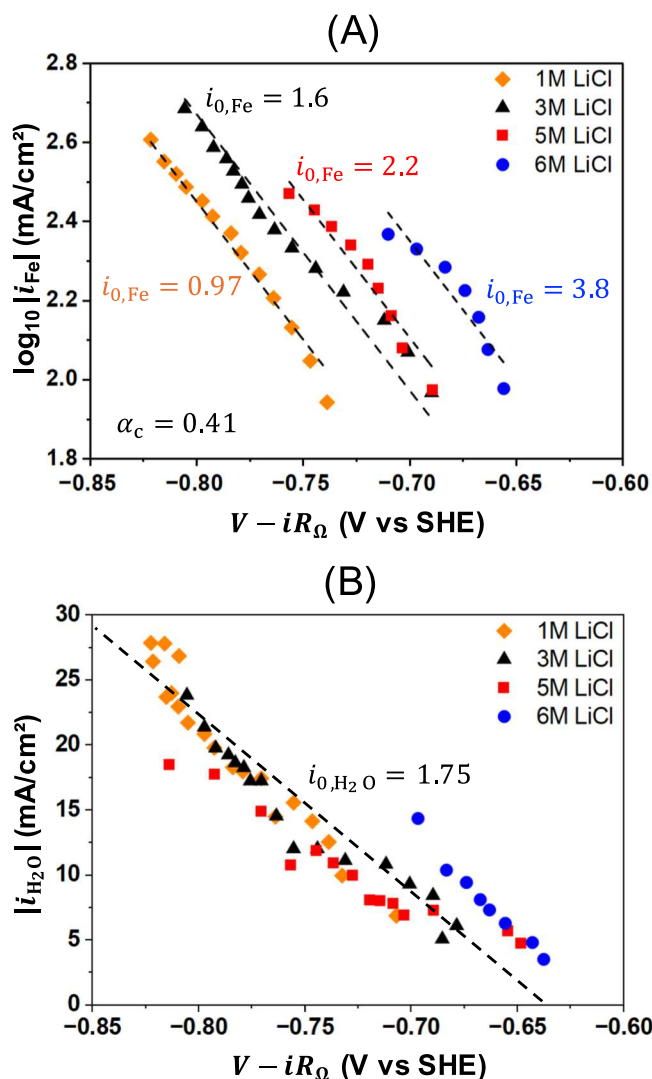


Figure 3. Kinetics analysis for electrolytes with 1 M FeCl₂, 0.01 M HCl and 1, 3, 5, or 6 M LiCl: (A) Tafel analysis of Fe deposition, indicating that LiCl primarily affects the exchange current density ($i_{0,\text{Fe}}$) but not the Tafel slope; (B) Water reduction reaction displays a linear relationship between $i_{\text{H}_2\text{O}}$ and potential, with $i_{0,\text{H}_2\text{O}}$ being relatively constant (1.75 mA cm⁻²). All potentials were iR_{Ω} -corrected using R_{Ω} from electrochemical impedance spectroscopy.

efficiency. This was also confirmed via gravimetric analysis of Fe deposits obtained after 5 min of plating from the 3 M LiCl electrolyte at 500 mA cm⁻², which provided a coulombic efficiency of 86.4% via Faraday's law, i.e., largely consistent with the coulometrically measured efficiency. To better understand the underlying mechanisms that determine the Fig. 1 trends, we now investigate the changes in kinetics and transport behavior of each reaction with increasing LiCl concentration.

Electrochemical analysis of partial currents followed the approach developed earlier by Sinclair et al.²⁴ Slow scan linear sweep voltammogram (5 mV s⁻¹) provided the polarization behavior on RDE (1000 RPM). The measured total current (i_{Total}) comprised of the iron plating partial current (i_{Fe}), the proton reduction current (i_{H}), and the water reduction current ($i_{\text{H}_2\text{O}}$). The proton reduction current was taken as its limiting value measured at positive electrode potentials (around -0.5 vs SHE) where iron plating and water reduction do not occur. At each applied current density i_{Total} , the iron plating partial current density i_{Fe} was available from the measured coulombic efficiencies (ϵ) from Fig. 1:

$$i_{\text{Fe}} = \epsilon i_{\text{Total}} \quad [1]$$

Current balance provides the water reduction partial current density $i_{\text{H}_2\text{O}}$ as:

$$i_{\text{H}_2\text{O}} = i_{\text{Total}} - i_{\text{H}} - i_{\text{Fe}} \quad [2]$$

The partial current densities were plotted as a function of the electrode potential in Fig. 2. For all LiCl concentrations (1 M, 3 M, 5 M, and 6 M), the water reduction current density remains much lower than the iron plating current density ($i_{\text{H}_2\text{O}} \ll i_{\text{Fe}}$). The kinetics of water reduction, as analyzed quantitatively below, do not show a significant dependence on the LiCl concentration. Finally, at large LiCl concentrations (i.e., 6 M), the iron plating exhibits a limiting current plateau signaling mass transport limitations congruent with an increase in $i_{\text{H}_2\text{O}}$. The transport limitations on Fe plating are due to sluggish diffusion of bulkier Fe²⁺-chloro-complexes that form as the LiCl concentration is increased. Some enhancement in transport of Fe²⁺ species due to H₂ gas-induced "mixing" is possible,³⁴⁻³⁶ but the limiting currents were largely consistent with Levich behavior indicating that such an effect was not dominant. The partial current densities in Fig. 2 now allow for a quantitative characterization of the effects of LiCl concentration on the kinetics behavior of the Fe electrodeposition and water reduction reactions.

Analysis of kinetics and modeling the deposition efficiency.—

The partial current densities from Fig. 2 were subjected to kinetics analysis. First, we constructed a Tafel plot (Fig. 3A) of i_{Fe} vs the potential ($V - iR_{\Omega}$),³⁷ and extracted the exchange current density for Fe deposition as a function of the LiCl concentration of the electrolyte. To avoid convolution from mass-transport effects, current density values in the vicinity of the Fe plating limiting current were excluded from the analysis.

$$\log_{10} |i_{\text{Fe}}| = \log_{10} i_{0,\text{Fe}} - \frac{\alpha_c F}{2.303RT} \times [V - E_{\text{Fe}} - iR_{\Omega}] \quad [3]$$

The iron reduction potential (E_{Fe}) was chosen as -0.447 V vs SHE. The charge transfer coefficient (α_c) was set to 0.41 for all curves in Fig. 3A since the Tafel slope seemed to be relatively constant irrespective of the LiCl concentration. Figure 3A suggests that an increase in LiCl concentration results in an increase in the Fe deposition exchange current density, i.e., $i_{0,\text{Fe}}$ increases by a factor of 4 going from 1 M LiCl to 6 M LiCl. This increase of $i_{0,\text{Fe}}$ also correlates with an observed visual color change of the electrolytes with increasing LiCl concentration indicating a complexation change of the Fe²⁺ species (supplementary materials, Fig. S1). For the water reduction reaction, $i_{\text{H}_2\text{O}}$ was plotted vs $V - iR_{\Omega}$, but a linear relationship was observed suggesting kinetics of the form:

$$i_{\text{H}_2\text{O}} = i_{0,\text{H}_2\text{O}} \frac{nF}{RT} (V - E_{\text{H}_2\text{O}} - iR_{\Omega}) \quad [4]$$

Figure 3B indicates $i_{0,\text{H}_2\text{O}}$ is close to 1.75 mA cm⁻² and that its value is relatively independent of the LiCl concentration of the electrolyte. This suggests that even 1 M LiCl sufficiently suppresses the reduction of water, hinting at a surface effect (e.g., adsorbed anions as suggested previously³⁹) underlying the kinetic suppression of water reduction. This observation is also consistent with the fact that 1 M and 3 M LiCl exhibit high Fe plating coulombic efficiencies (>90%) at high current densities (Fig. 1).

The measurement of the kinetic constants $i_{0,\text{Fe}}$ and $i_{0,\text{H}_2\text{O}}$ now allow us to model the deposition efficiency as a function of the current density. By definition, the coulombic efficiency is:

$$\varepsilon = \frac{i_{\text{Fe}}}{i_{\text{Fe}} + i_{\text{H}_2\text{O}} + i_{\text{H}}} \quad [5]$$

Here, $i_{\text{H}_2\text{O}}$ and i_{Fe} are computed using:

$$i_{\text{Fe}} = i_{0,\text{Fe}} \left(1 - \frac{i_{\text{Fe}}}{i_{\text{L,Fe}}} \right) \exp \left[\frac{\alpha_c F}{RT} (V - E_{\text{Fe}}) \right] \quad [6]$$

$$i_{\text{H}_2\text{O}} = i_{0,\text{H}_2\text{O}} \frac{nF}{RT} (V - E_{\text{H}_2\text{O}}) \quad [7]$$

The transport-limited H^+ reduction current density i_{H} (in Eq. 5), and the transport-limited Fe^{2+} reduction current density $i_{\text{L,Fe}}$ (in Eq. 6) were available from direct experimental observations (Fig. 2). Note here that Eq. 6 includes a standard modification to account for mass transport limitations at high rates where i_{Fe} approaches $i_{\text{L,Fe}}$. All partial currents add up to i_{Total} , thus:

$$i_{\text{Total}} = i_{\text{Fe}} + i_{\text{H}_2\text{O}} + i_{\text{H}} \quad [8]$$

For a given i_{Total} , Eqs. 5–8 can be solved to obtain i_{Fe} , $i_{\text{H}_2\text{O}}$, V , and ε . A plot of ε vs i_{Total} is provided in Fig. 4 for electrolytes containing 3 M LiCl (Fig. 4A) and 5 M LiCl (Fig. 4B). First, a reasonable agreement with the experimentally observed trends (from Fig. 1) is noted. The discontinuity seen in the modeled ε trends around i_{Total} of about 100 mA cm^{-2} is due to the onset of water reduction. However, despite onset of water reduction current ($i_{\text{H}_2\text{O}}$), the overall ε is maintained at a high level (>90% in regime 2) because the Fe plating rate (i_{Fe}) increases exponentially with potential (Eq. 6), whereas water reduction increases only linearly with potential (Eq. 7). It is only when the Fe plating rate approaches its limiting value $i_{\text{L,Fe}}$ that $i_{\text{H}_2\text{O}}$ begins to dominate the total current, causing a drop in ε , as noticed clearly in Fig. 4B on account of the more viscous nature of the 5 M LiCl-containing electrolyte. This modeling study not only provides a more quantitative basis for the efficiency trends observed in Fig. 1, but also enables modeling-based prediction of the optimal operating conditions (LiCl concentration, i_{Total}) for efficient Fe plating.

Electrolyte speciation controls diffusion and kinetics properties.—To visualize the trends in transport and kinetics properties, the Fe^{2+} diffusion coefficients (obtained from Levich analysis of the limiting oxidation currents on RDE), and the iron deposition and water reduction exchange current densities (from Fig. 3) were plotted as

function of the total Cl^- content of the electrolytes (Figs. 5A and 5B). In addition, a speciation study was performed to map the mole fractions of the various iron species (Fe^{2+} , FeCl_4^{2-} , FeCl_2 , and FeCl^+) in the electrolytes, using stability constants available in literature,³¹ as shown in Fig. 5C. For a fixed and known Cl^- concentration, equations in Table I can be solved to determine the concentrations of the various Fe^{2+} complexes for an assumed total Fe content of 1 M.

It is observed from Fig. 5C that increasing the Cl^- concentration leads to increased chloro-complexation of the Fe^{2+} . At low Cl^- concentration (<4 M), the uncomplexed Fe^{2+} dominates. At moderate Cl^- concentrations (>4 M), the FeCl^+ complex concentration gradually increases above that of the uncomplexed Fe^{2+} . But, at very high Cl^- concentration (8 M), the FeCl_4^{2-} complex becomes the dominant species in the electrolyte. The uncomplexed Fe^{2+} exhibits the lowest $i_{0,\text{Fe}}$ (Fig. 5B), while having the largest diffusion coefficient (Fig. 5A). At moderate Cl^- concentrations, $i_{0,\text{Fe}}$ increases somewhat with Cl^- concentration but $i_{0,\text{H}_2\text{O}}$ remains unchanged together with a gradual decrease in Fe^{2+} diffusivity. But, in the highly FeCl^+ complexed electrolyte, $i_{0,\text{Fe}}$ increases markedly while the Fe^{2+} -complex diffusion coefficient drops abruptly. These trends are key to explaining the experimental efficiency data (Fig. 1):

- (i) 1 M LiCl (or 3 M total Cl^-): Fe plating is sluggish, leading to generally low plating efficiency.
- (ii) 3–5 M LiCl (or 5–7 M total Cl^-): FeCl^+ complexes begin to form which accelerate Fe plating while keeping water reduction suppressed, leading to high plating efficiencies.
- (iii) 6 M LiCl (or 8 M total Cl^-): FeCl_4^{2-} complexes dominate but these have sluggish diffusional transport properties, hence the overall plating efficiency is lowered at high current densities.

Effects of Li^+ and Cl^- in modulating deposition and HER.—The cation (Li^+) and anion (Cl^-) play specific roles in accelerating iron deposition kinetics and suppressing water reduction. To gain further insights into the anion and cation effects, we switched Li^+ to potassium (K^+) and Cl^- to perchlorate (ClO_4^-) in the electrolytes to investigate how these species affect the kinetics of Fe deposition and water reduction. The coulombic efficiency was measured and used to deconvolute the polarization behavior into partial currents i_{Fe} and $i_{\text{H}_2\text{O}}$ following procedure analogous to Figs. 1–3. Summary of findings is shown in Fig. 6 for electrolytes containing 1 M FeY_2 , 0.01 M HY, and 3 M XY (where X = Li^+ or K^+ , and Y = Cl^- or ClO_4^-). Perchlorate anion was chosen because it does not adsorb³⁸ and does not complex³⁹ with iron. Also, potassium was chosen as a

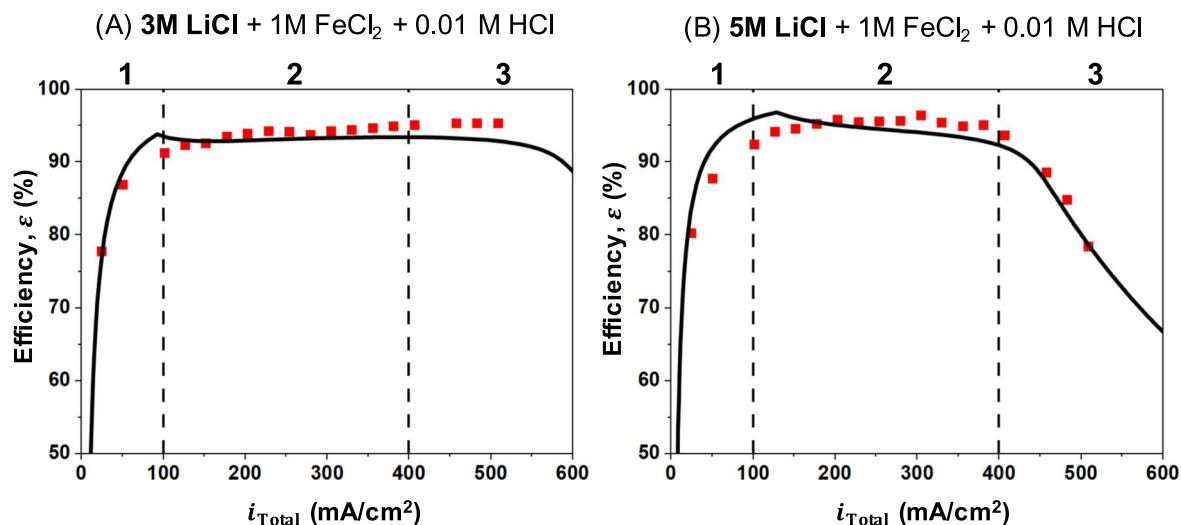


Figure 4. Efficiency of Fe plating obtained from solving Eqs. 5–8 for electrolytes containing 1 M FeCl_2 , 0.01 M HCl and either 3 M LiCl (A) or 5 M LiCl (B). Good agreement with experimental efficiency values is noted. Regimes 1, 2 and 3 correspond to current ranges in Fig. 1.

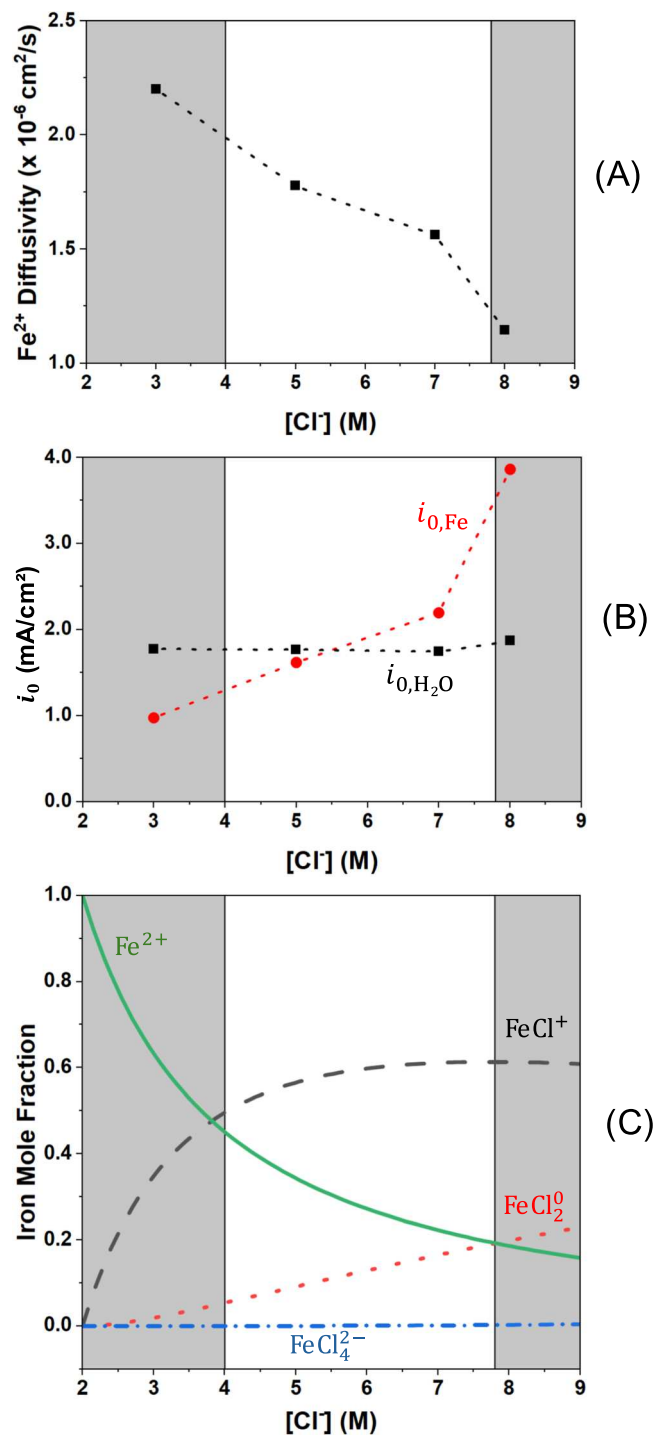


Figure 5. Fe^{2+} diffusivity (A), iron deposition and water reduction exchange current densities (B), and iron speciation (C) as a function of the total chloride concentration of electrolytes. The Fe^{2+} diffusivity drops markedly and $i_{0,Fe}$ increases considerably as total $[Cl^-]$ approaches 8 M, due to formation of $FeCl^+$ complexes.

substitute for Li^+ because it is a larger cation that is reported in literature to enhance water reduction kinetics in alkaline electrolytes compared to Li^+ .²⁵

Figure 6A illustrates why both Li^+ and Cl^- are key to achieving a high Fe deposition coulombic efficiency. The ClO_4^- based electrolyte has a maximum plating efficiency of 70% (well below that with $LiCl$), whereas the K^+ based electrolyte provides efficiency approaching 90% (also lower than with $LiCl$). Kinetic analysis of the

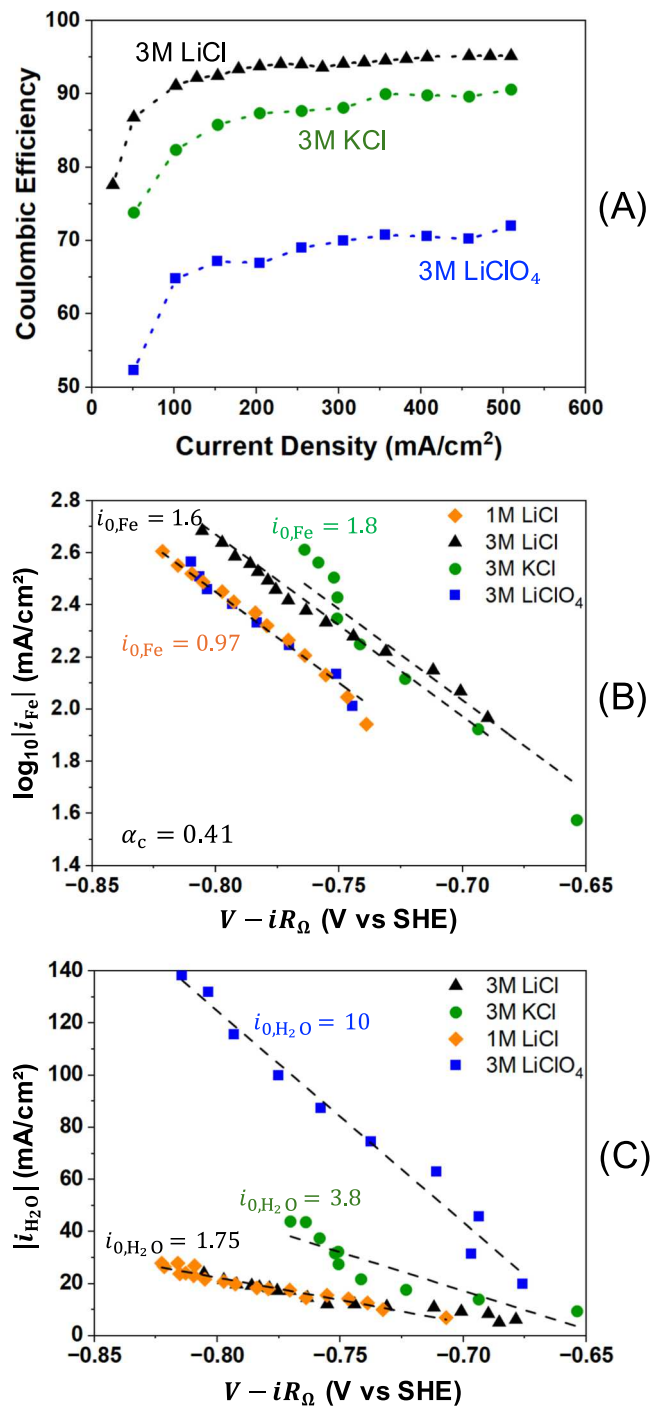


Figure 6. (A) Effect of anion and cation choice on the Fe deposition coulombic efficiency for electrolytes containing 1 M FeY_2 , 0.01 M HY, and 3 M XY (where X = Li^+ or K^+ , and Y = Cl^- or ClO_4^-). Replacing Li^+ with K^+ or Cl^- with ClO_4^- lowers efficiency. (B) Tafel analysis of i_{Fe} indicates that ClO_4^- anion does not enhance Fe plating kinetics and that high Cl^- concentrations are needed for enhancing $i_{0,Fe}$. (C) Water reduction reaction is not effectively suppressed by K^+ or ClO_4^- , explaining why both Li^+ and Cl^- are necessary for enhancing efficiency.

polarization data (Figs. 6B and 6C) reveals interesting trends in the values of $i_{0,Fe}$ and i_{0,H_2O} . For 3 M KCl , the value of $i_{0,Fe}$ (for a fixed cathodic transfer coefficient of 0.41) was similar to that when using 3 M $LiCl$ (1.6–1.8 mA cm^{-2}). In contrast, this value dropped to 0.97 mA cm^{-2} when using 3 M $LiClO_4$, suggesting the key role of Cl^- in maintaining high Fe plating kinetics from chloro-complexes. The

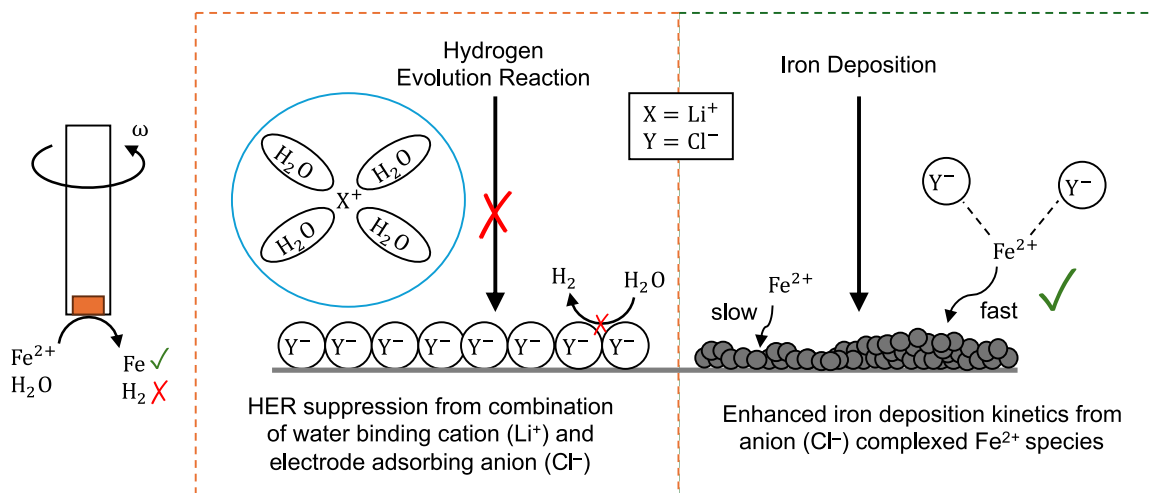


Figure 7. Schematic depicting a mechanism through which cation (Li^+) and anion (Cl^-) selection enable highly efficient (>90%) Fe plating electrolytes operating at high current densities.

Table I. Formulae used for complexation calculations in Fig. 5C, and the associated values of complexation constants.

Equation	Complexation constants ³¹
$\beta_1 = \frac{[\text{FeCl}^+]}{[\text{Fe}^{2+}][\text{Cl}^-]}$	$\log(\beta_1) = -0.366$
$\beta_2 = \frac{[\text{FeCl}_2]}{[\text{Fe}^{2+}][\text{Cl}^-]^2}$	$\log(\beta_2) = -1.74$
$\beta_4 = \frac{[\text{FeCl}_4^{2-}]}{[\text{Fe}^{2+}][\text{Cl}^-]^4}$	$\log(\beta_4) = -5.41$
$[\text{Fe}^{2+}] = 1 - [\text{FeCl}_4^{2-}] - [\text{FeCl}^+] - [\text{FeCl}_2]$	N/A

effect of cation and anion on the water reduction exchange current density was even more pronounced. The value of $i_{0,\text{H}_2\text{O}}$ increased considerably from 1.75 mA cm^{-2} to 3.8 mA cm^{-2} for 3 M LiCl and KCl, respectively, and it increased to 10 mA cm^{-2} for 3 M LiClO₄. This underscores the importance of Li^+ and more importantly Cl^- in collectively suppressing water reduction and providing maximal Fe plating efficiency at high rates.

Literature reports suggest that smaller cations (i.e., Li^+) are less surface-bound in comparison to larger cations (i.e., K^+),⁴⁰ and this helps suppress HER kinetics with Li^+ because surface-bound cations facilitate easier dissociation of water.^{25,41} On the other hand, the $i_{0,\text{Fe}}$ for both 3 M LiCl and 3 M KCl are similar, indicating a similar chloro-complex (FeCl^+) is forming and that the cation of the supporting electrolyte (Li^+ vs K^+) does not play a major role in modulating Fe deposition kinetics. Preventing chloro-complexes of Fe^{2+} by employing ClO_4^- as the anion suppresses Fe plating kinetics, further highlighting the key role of Cl^- .

The unique role of the anion (Cl^-) in surface adsorption mediated HER suppression²⁹ and accelerating plating kinetics via Fe^{2+} chloro-complex formation, and that of the cation (Li^+) in avoiding surface-enhancement of HER is depicted schematically in Fig. 7. Unlike larger cations that surface adsorb onto the electrode surface, a cation that coordinates with water, such as Li^+ in high enough concentrations, will bind up the water and prevent it from reaching to the surface. Since the surface adsorbing anion does not need to compete with cation adsorption, it can prevent hydrogen adsorption and thus suppress HER. Iron deposition kinetics increase via a complexing anion such as Cl^- that replaces water within Fe^{2+} solvation but does not complex strongly enough to prevent deposition.

Conclusions

Judicious selection of cation and anion species in the supporting electrolyte enables efficient iron electrodeposition at high current densities. For LiCl-containing Fe deposition electrolytes, efficient plating is enabled by Li^+ and Cl^- playing unique roles. The Li^+ and Cl^- effectively suppresses water reduction. Additionally, the Cl^- promotes formation of Fe^{2+} chloro-complexes which exhibit high exchange current densities for Fe deposition. These effects together lead to a current-efficient Fe plating process. The proposed LiCl-containing electrolytes achieved superior coulombic efficiency (>90%) at industrially-relevant current densities (>400 mA cm^{-2}), making them attractive not only for high-volume iron metal electro-synthesis but also for grid-scale energy storage in the form of iron-based redox flow batteries.

Acknowledgments

This work was supported as part of the Center for Steel Electrification by Electrosynthesis (C-STEEL), an Energy Earthshot Research Center funded by the U.S. Department of Energy, Office of Science, Basic Energy Sciences (BES) and Advanced Scientific Computing Research (ASCR).

ORCID

William Lvovich <https://orcid.org/0009-0001-6349-9596>
 Nicholas Sinclair <https://orcid.org/0000-0002-8268-966X>
 Justin G. Connell <https://orcid.org/0000-0002-2979-2131>
 Rohan Akolkar <https://orcid.org/0000-0002-9865-5704>

References

- National Minerals Information Center, *Iron and Steel Statistics and Information* (USGS) <https://usgs.gov/centers/national-minerals-information-center/iron-and-steel-statistics-and-information> (accessed 6/23/2025).
- Z. Fan and S. J. Friedmann, "Low-carbon production of iron and steel: Technology options, economic assessment, and policy," *Joule*, **5**, 829 (2021).
- J. Kim, B. K. Sovacool, M. Bazilian, S. Griffiths, J. Lee, M. Yang, and J. Lee, "Decarbonizing the iron and steel industry: A systematic review of sociotechnical systems, technological innovations, and policy options," *Energy Research & Social Science*, **89**, 102565 (2022).
- NIH, *Considerations for the Use of Unencapsulated Steel Slag* (National Academies Press) (2023), <https://ncbi.nlm.nih.gov/books/NBK599051/> accessed 6/23/2025.
- A. Badalbayli, N. Sinclair, E. Kim, A. A. Baker, and R. Akolkar, "Editors' choice— Molten salt electrolysis in chloride melts for energy-efficient iron metal production," *J. Electrochem. Soc.*, **172**, 032508 (2025).
- Boston Metal, *About Boston Metal* (2025), <https://bostonmetal.com/about/> (accessed 6/23/2025).
- C. Stinn and A. Allamore, "Estimating the capital costs of electro-winning processes," *The Electrochemical Society Interface*, **29**, 44 (2020).

8. A. Allanore, L. Yin, and D. R. Sadoway, "A new anode material for oxygen evolution in molten oxide electrolysis." *Nature*, **497**, 353 (2013).
9. A. Allanore, "Features and challenges of molten oxide electrolytes for metal extraction." *J. Electrochem. Soc.*, **162**, E13 (2014).
10. M. Esmaily, A. N. Mortazavi, N. Birbilis, and A. Allanore, "Oxidation and electrical properties of chromium-iron alloys in a corrosive molten electrolyte environment." *Sci. Rep.*, **10**, 14833 (2020).
11. A. Badalbayli, N. Sinclair, R. Bernasconi, N. Borisenko, K. Venkatesh, A. Ispas, R. Akolkar, and L. Magagnin, "Advancements in electrodeposition for precise manufacturing and sustainability." *The Electrochemical Society Interface*, **33**, 47 (2024).
12. B. Beverskog and I. Puigdomenech, "Revised Pourbaix diagrams for iron at 25–300 °C." *Corros. Sci.*, **38**, 2121 (1996), Revised pourbaix diagrams for iron at 25–300°C.
13. S. Koutsoupa, S. Koutalidi, E. Balomenos, and D. Panias, "SIDERWIN—a new route for iron production." *Materials Proceedings*, **5**, 58 (2021).
14. A. Konovalova, A. C. Goldman, R. Shekhar, I. Triplett, L. J. Moutarlier, M. Kwak, and P. A. Kempler, "Pathways to electrochemical ironmaking at scale via the direct reduction of Fe₂O₃." *ACS Energy Lett.*, **10**, 1851 (2025).
15. B. B. Noble, A. Konovalova, L. J. Moutarlier, V. Brogden, and P. A. Kempler, "Electrochemical chlor-iron process for iron production from iron oxide and salt water." *Joule*, **8**, 714 (2024).
16. Electra, *Our Technology* (2025), <https://electra.earth/our-technology/> (accessed 6/23/2025).
17. A. Q. Pham, S. Nijhawan, A. Alvarez, and S. Fatur, "Ore dissolution and iron conversion system." (2023), US11753732B2.
18. T. Braun, C. Wallace, Q. Pham, S. Nijhawan, and C. L. Alexander, "Electrochemistry in action: iron and steel manufacturing." *The Electrochemical Society Interface*, **33**, 38 (2024).
19. P. C. Pistorius, "Energy requirements for electrification of ironmaking and steelmaking." *South African Pyrometallurgy* (The South African Institute of Mining and Metallurgy, Johannesburg, South Africa) (2024).
20. L. Suo, O. Borodin, T. Gao, M. Olguin, J. Ho, X. Fan, C. Luo, C. Wang, and K. Xu, "'Water-in-salt' electrolyte enables high-voltage aqueous lithium-ion chemistries." *Science*, **350**, 938 (2015).
21. L. Chen et al., "A 63m superconcentrated aqueous electrolyte for high-energy Li-ion batteries." *ACS Energy Lett.*, **5**, 968 (2020).
22. J. Liu, D. Dong, A. L. Caro, N. S. Andreas, Z. Li, Y. Qin, D. Bedrov, and T. Gao, "Aqueous electrolytes reinforced by Mg and Ca ions for highly reversible Fe metal batteries." *ACS Central Science*, **8**, 729 (2022).
23. L. C. Greenburg, J. Holoubek, Y. Cui, P. Zhang, H. Ai, E. Zhang, C. Liu, G. Feng, and Y. Cui, "Crowding agent stabilizes aqueous electrolyte for reversible iron metal anode." *ACS Energy Lett.*, **10**, 1022 (2025).
24. N. S. Sinclair, J. Luo, K. Park, M. Oakes, B. Martin, A. Balakrishnan, J. G. Connell, D. Kang, and R. Akolkar, "Choline chloride-based water-in-salt electrolyte for efficient iron electrodeposition." *J. Electrochem. Soc.*, **172**, 062503 (2025).
25. J. T. Bender, A. S. Petersen, F. C. Østergaard, M. A. Wood, S. M. J. Heffernan, D. J. Milliron, J. Rossmeis, and J. Resasco, "Understanding cation effects on the hydrogen evolution reaction." *ACS Energy Lett.*, **8**, 657 (2022).
26. S. Xue, B. Garlyyev, S. Watzel, Y. Liang, J. Fichtner, M. D. Pohl, and A. S. Bandarenka, "Influence of alkali metal cations on the hydrogen evolution reaction activity of Pt, Ir, Au, and Ag electrodes in alkaline electrolytes." *Chem. Electrochem.*, **5**, 2326 (2018).
27. M. C. O. Monteiro, A. Goyal, P. Moerland, and M. T. M. Koper, "Understanding cation trends for hydrogen evolution on platinum and gold electrodes in alkaline media." *ACS Catal.*, **11**, 14328 (2021).
28. G. Gao, G. Zhao, G. Zhu, B. Sun, Z. Sun, S. Li, and Y.-Q. Lan, "Recent advancements in noble-metal electrocatalysts for alkaline hydrogen evolution reaction." *Chin. Chem. Lett.*, **36**, 109557 (2025).
29. K. L. Hawthorne, T. J. Petek, M. A. Miller, J. S. Wainright, and R. F. Savinell, "An investigation into factors affecting the iron plating reaction for an all-iron flow battery." *J. Electrochem. Soc.*, **162**, A108 (2014).
30. D. Shen, M. B. Vukmirovic, and R. Akolkar, "Understanding the role of complexation in the charge-transfer kinetics of the Cu²⁺ + e ↔ Cu¹⁺ redox reaction in ethaline deep eutectic solvent." *J. Electrochem. Soc.*, **166**, E526 (2019).
31. R. Zhao and P. Pan, "A spectrophotometric study of Fe(II)-chloride complexes in aqueous solutions from 10 to 100 °C." *Can. J. Chem.*, **79**, 131 (2011).
32. A. J. Bard and L. R. Faulkner, *Electrochemical Methods: Fundamentals and Applications* (Wiley, New York) (2001).
33. S. De, J. White, T. Brusuelas, C. Patton, A. Koh, and Q. Huang, "Electrochemical behavior of protons and cupric ions in water in salt electrolytes with alkaline metal chloride." *Electrochim. Acta*, **338**, 135852 (2020).
34. D. W. Dees and C. W. Tobias, "Mass transfer at gas evolving surfaces: a microscopic study." *J. Electrochem. Soc.*, **134**, 1702 (1987).
35. C. Gabrielli, F. Huet, and R. P. Nogueira, "Fluctuations of concentration overpotential generated at gas-evolving electrodes." *Electrochim. Acta*, **50**, 3726 (2005).
36. D. P. Sutija and C. W. Tobias, "Mass-transport enhancement by rising bubble curtains." *J. Electrochem. Soc.*, **141**, 2599 (1994).
37. X. Shen, N. Sinclair, J. Wainright, and R. F. Savinell, "Methods—Analyzing electrochemical kinetic parameters in deep eutectic solvents using an extended Butler-Volmer equation." *J. Electrochem. Soc.*, **168**, 056520 (2021).
38. L. Ciavatta and M. Grimaldi, "On the hydrolysis of the iron(III) ion, Fe³⁺, in perchlorate media." *J. Inorg. Nucl. Chem.*, **37**, 163 (1975).
39. J. H. Kim, J. H. Lee, R. R. Palem, M.-S. Suh, H. H. Lee, and T. J. Kang, "Iron (II/III) perchlorate electrolytes for electrochemically harvesting low-grade thermal energy." *Sci. Rep.*, **9**, 8706 (2019).
40. G. K. Gebremariam, A. Z. Jovanović, I. A. Pašti, G. K. Gebremariam, A. Z. Jovanović, and I. A. Pašti, "The effect of electrolytes on the kinetics of the hydrogen evolution reaction." *Hydrogen*, **4**, 776 (2023).
41. B. Huang et al., "Cation- and pH-dependent hydrogen evolution and oxidation reaction kinetics." *JACS Au*, **1**, 1674 (2021).